Supplementary Information (SI) for Journal of Materials Chemistry A.

Electronic Supplementary Information

A multifunctional polymer to enhance SEI stability and Li utilization for efficient lithium metal batteries

Qiong Wang et al.

Table of Contents

Section 1: Supplementary Characterization Result Fig. S1-S25

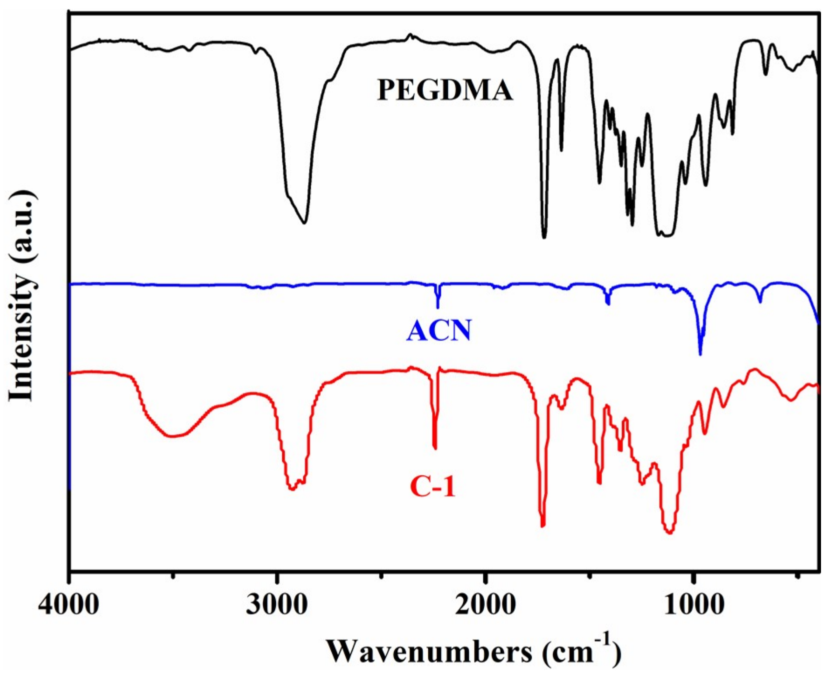

Fig. S1 FTIR spectra of PEGDMA, ACN and polymer C-1.

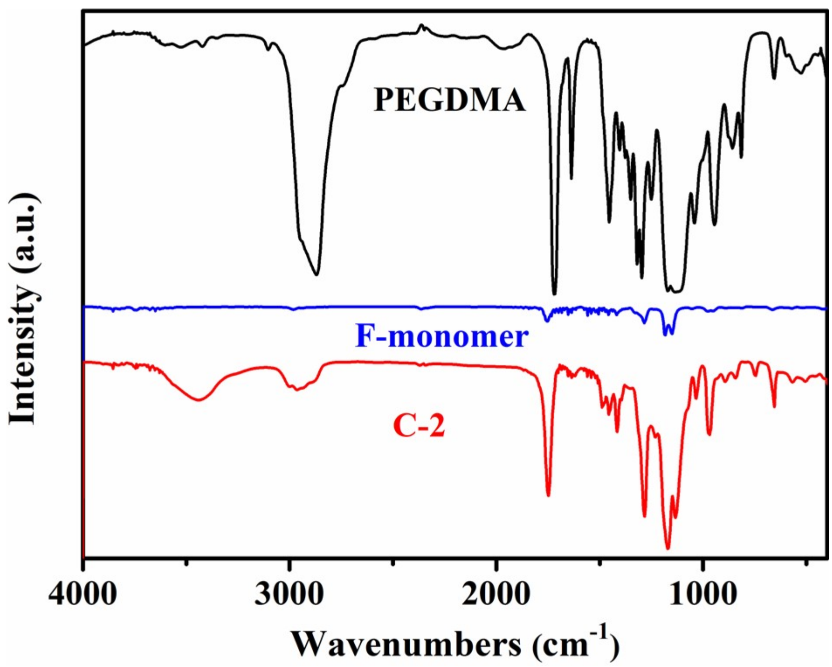

Fig. S2 FTIR spectra of PEGDMA, F-monomer and polymer C-2.

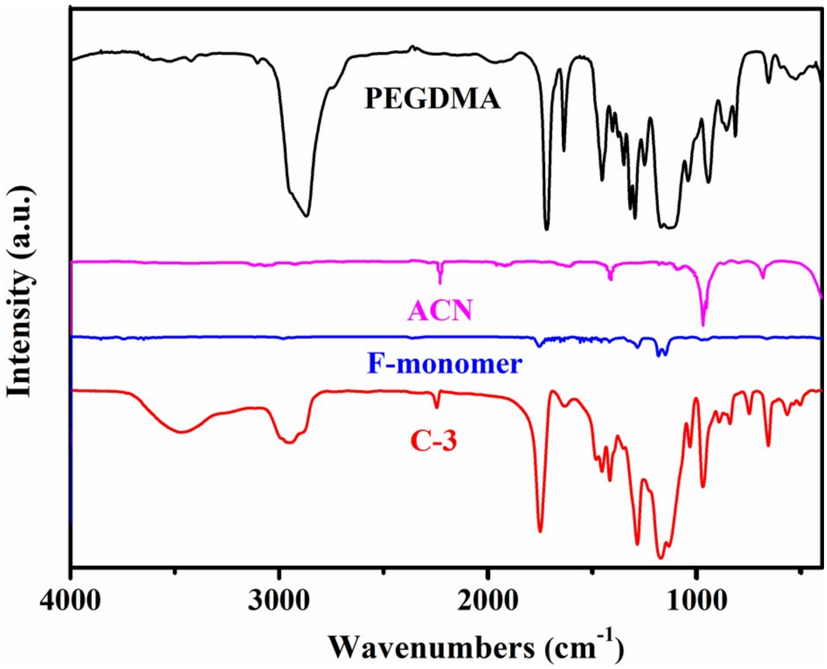

Fig. S3 FTIR spectra of PEGDMA, ACN, F-monomer and polymer C-3.

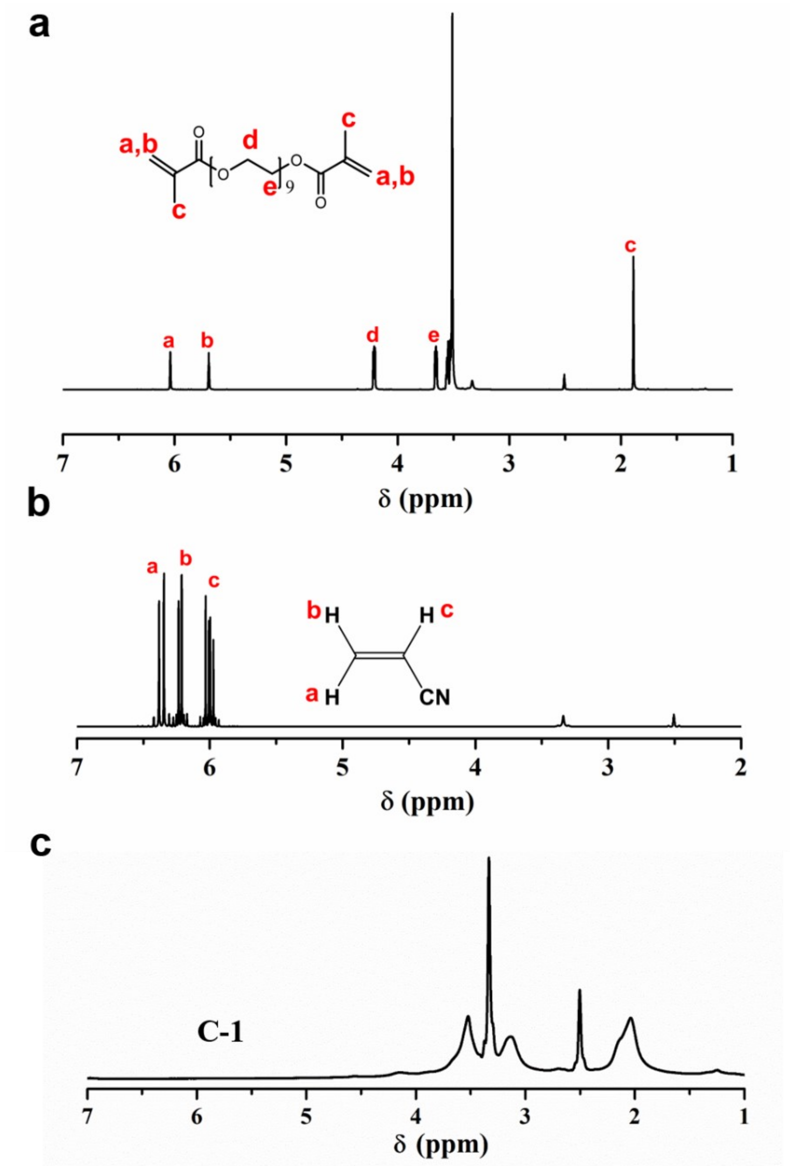

Fig. S4 ^{1}H NMR spectra of (a) PEGDMA, (b) ACN and (c) polymer C-1.

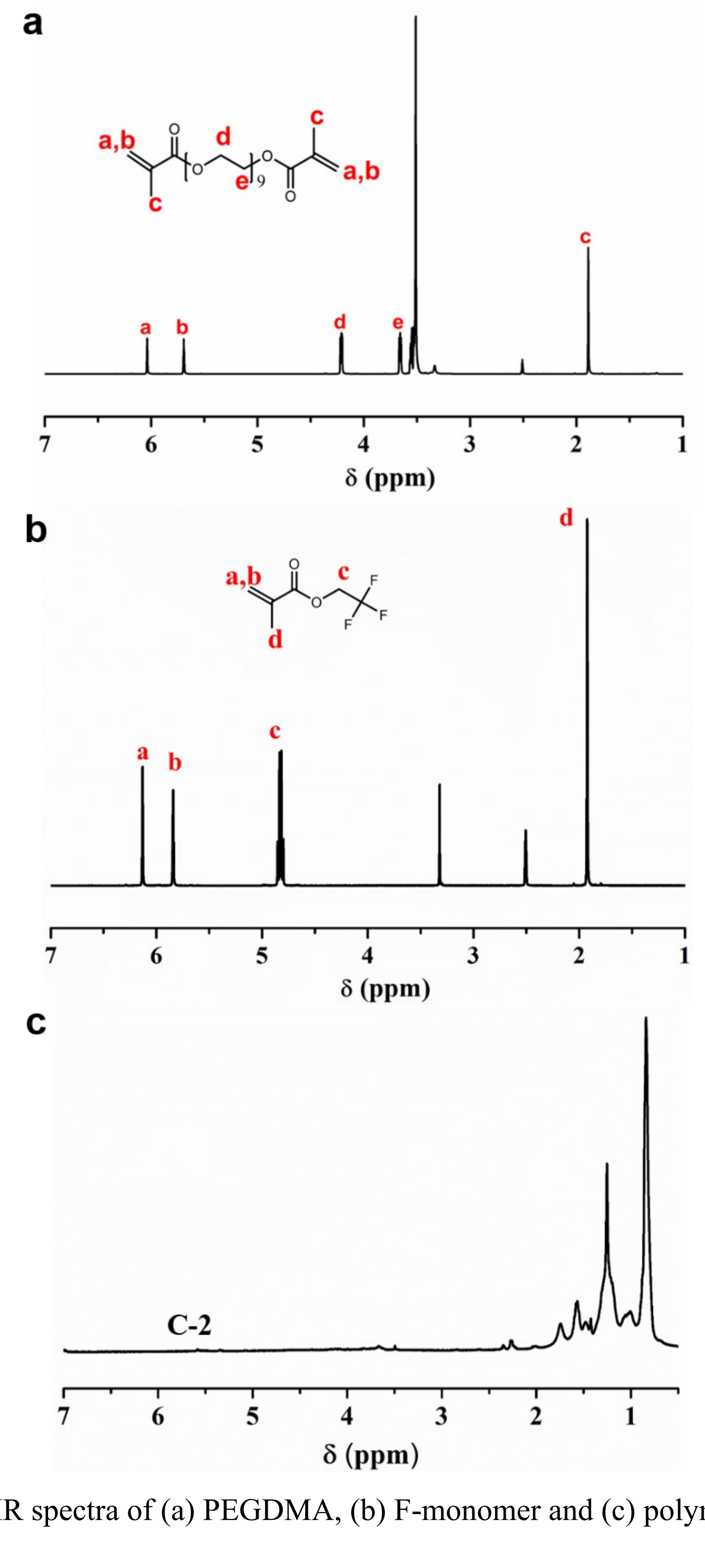

Fig. S5 [1]H NMR spectra of (a) PEGDMA, (b) F-monomer and (c) polymer C-2.

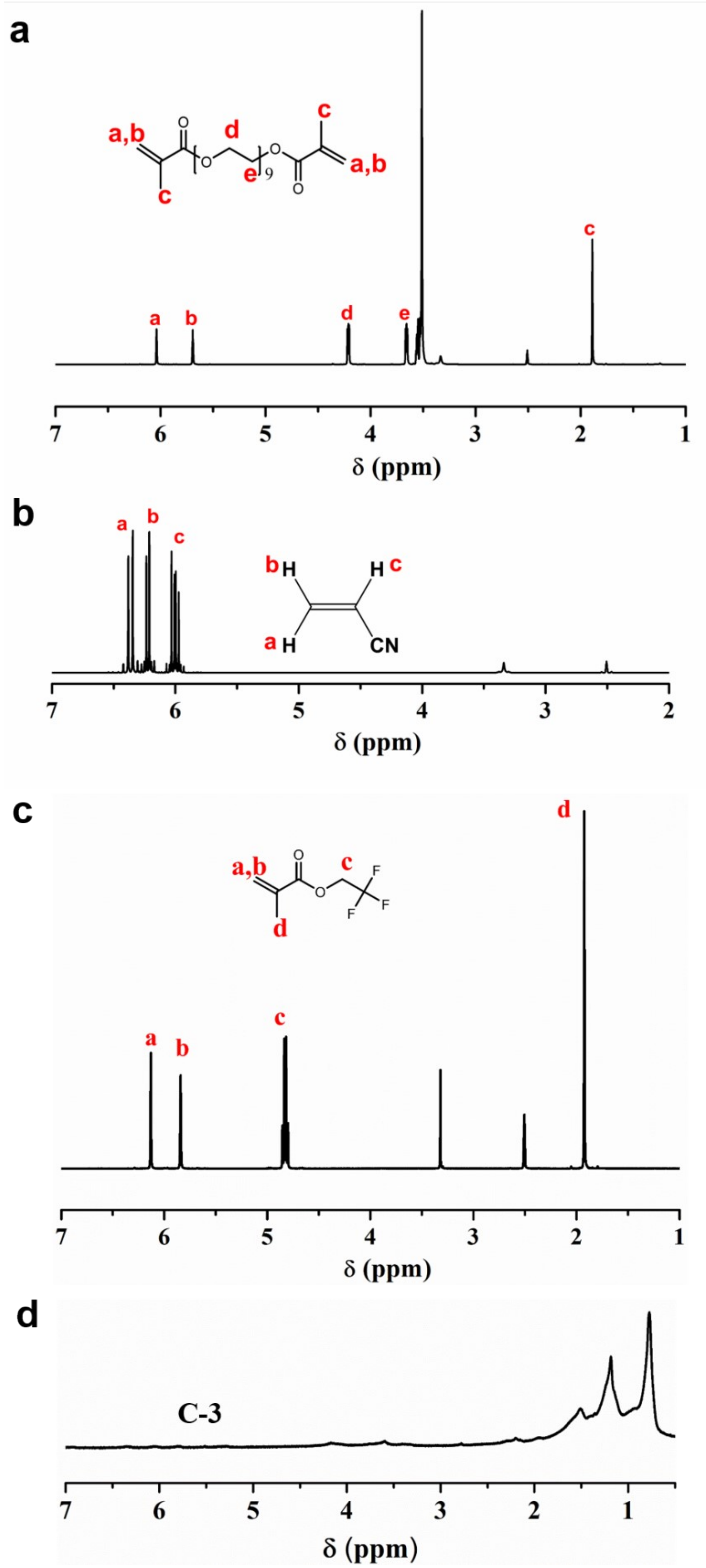

Fig. S6 [1]H NMR spectra of (a) PEGDMA, (b) ACN, (c) F-monomer and (d) polymer C-3.

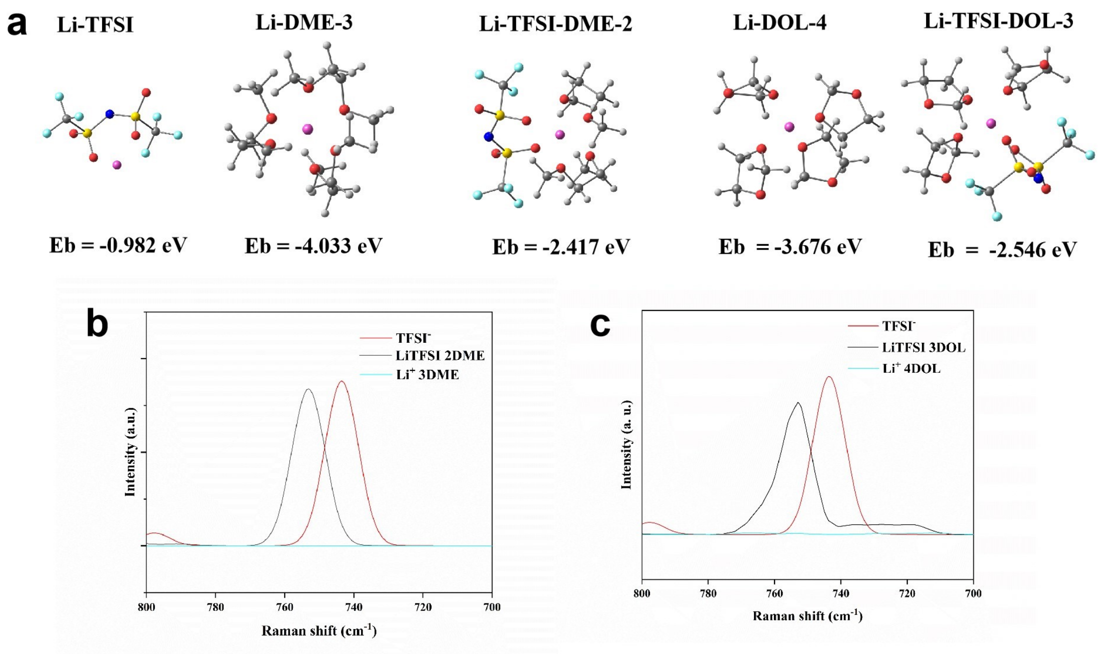

Fig. S7 (a) Calculation of Li^+ solvation clusters in ether-based electrolyte. Calculated Raman spectra of Li^+ solvation clusters with (b) DME and (c) DOL molecules.

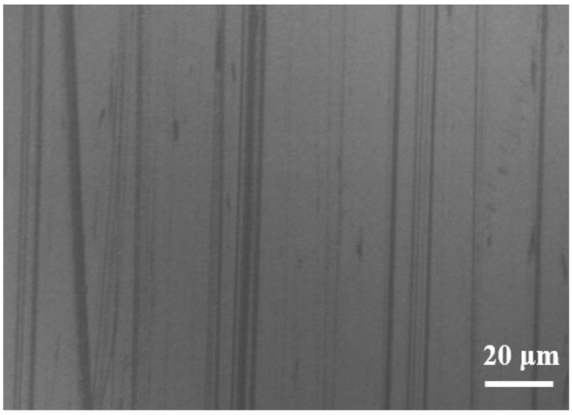

Fig. S8 SEM image of PP separator surface without polymer modification.

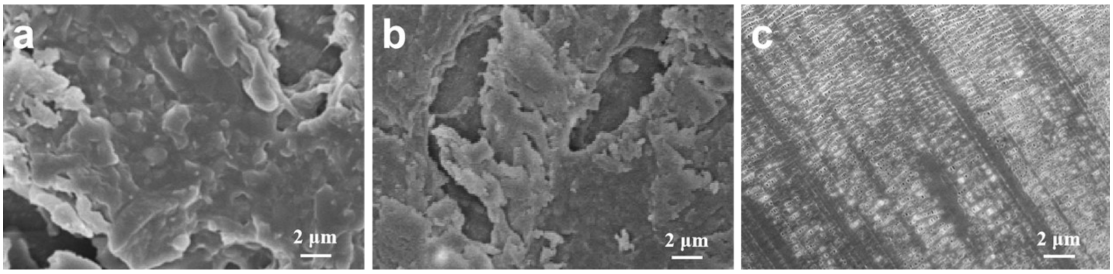

Fig. S9 Morphological analysis of the C-3-modified PP separators. SEM image of PP surface with (a) 12.4 mg, (b) 9.5 mg and (c) 6.7 mg coating loading.

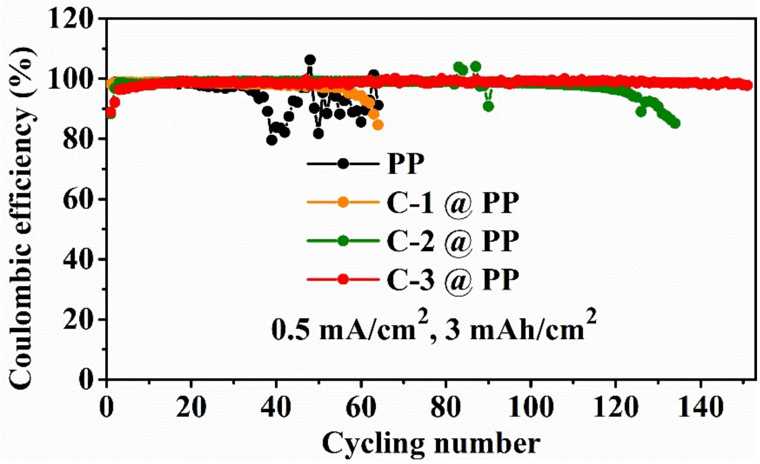

Fig. S10 Coulombic efficiency of the Li/Cu batteries in ether-based electrolyte assembled with PP, C-1-modified, C-2-modified and C-3-modified PP separators at a current density of 0.5 mA/cm^2 with a cycling capacity of 3 mAh/cm^2.

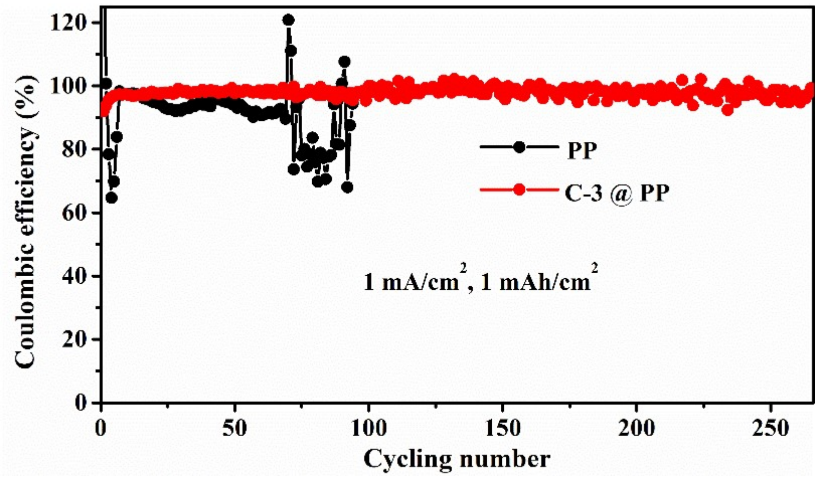

Fig. S11 Coulombic efficiency of the Li/Cu batteries in ether-based electrolyte assembled with PP and C-3-modified PP separators at a current density of 1 mA/cm^2 with a cycling capacity of 1 mAh/cm^2.

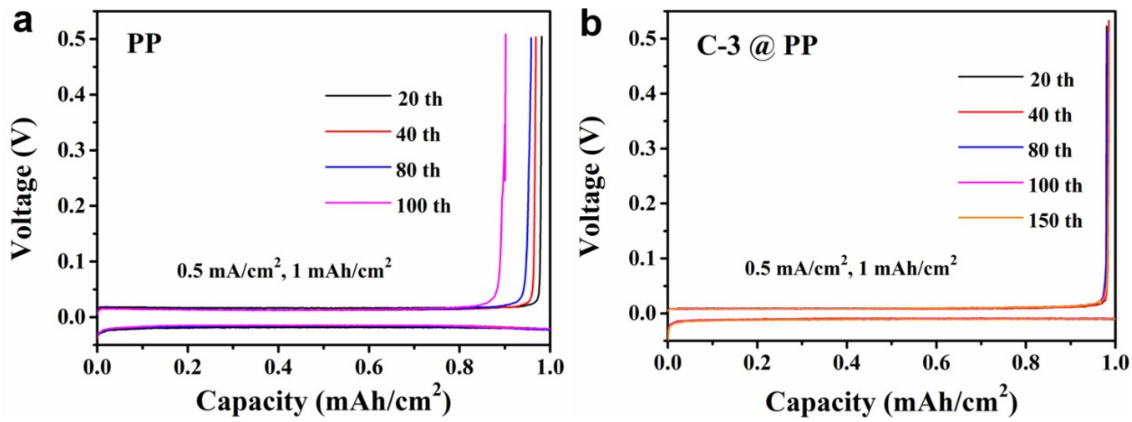

Fig. S12 The corresponding voltage profiles of Li/Cu batteries in ether-based electrolyte with (a) PP separator and (b) C-3-modified PP separator at a current density of 0.5 mA/cm^2 with a cycling capacity of 1 mAh/cm^2.

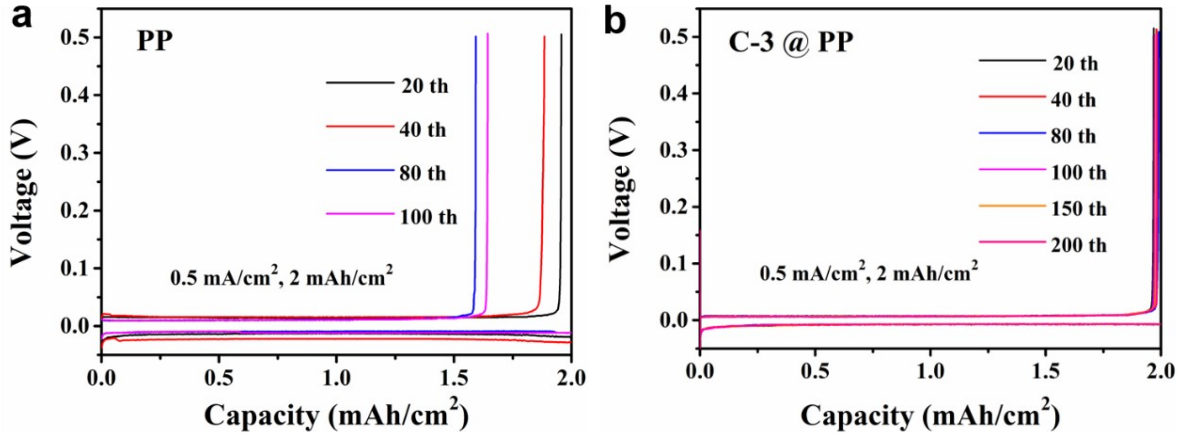

Fig. S13 The corresponding voltage profiles of Li/Cu batteries in ether-based electrolyte with (a) PP separator and (b) C-3-modified PP separator at a current density of 0.5 mA/cm^2 with a cycling capacity of 2 mAh/cm^2.

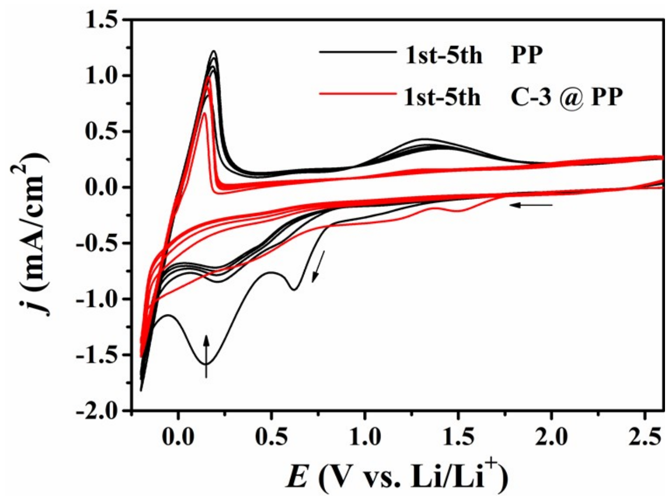

Fig. S14 Cyclic voltammetry (CV) curves of the Li/Cu batteries with the electrolyte composed of 1 M LiTFSI/DME–DOL (volume ratio 1:1) with 1% $LiNO_3$ using pristine PP and C-3-modified PP separators respectively at a scan rate of 50 mV/s in the first five cycles.

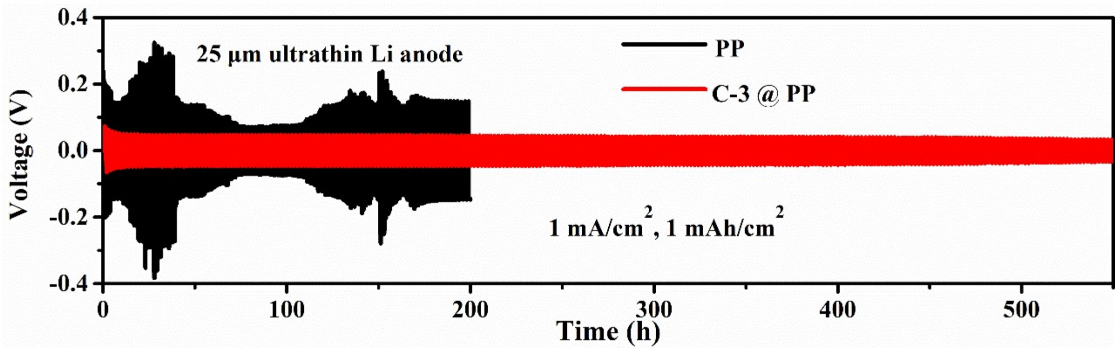

Fig. S15 Performance of Li/Li symmetric batteries in ether-based electrolyte using 25 μm ultra-thin Li anodes. Cycling stability comparison of the batteries assembled with PP and C-3-modified PP separators at a current density of 1 mA/cm^2 with a cycling capacity of 1 mAh/cm^2.

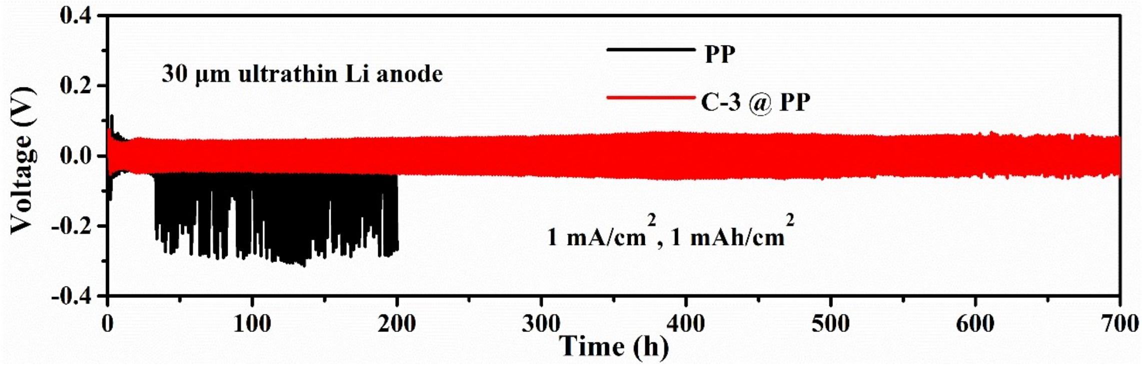

Fig. S16 Performance of Li/Li symmetric batteries in ether-based electrolyte using 30 μm ultra-thin Li anodes. Cycling stability comparison of the batteries assembled with PP and C-3-modified PP separators at a current density of 1 mA/cm^2 with a cycling capacity of 1 mAh/cm^2.

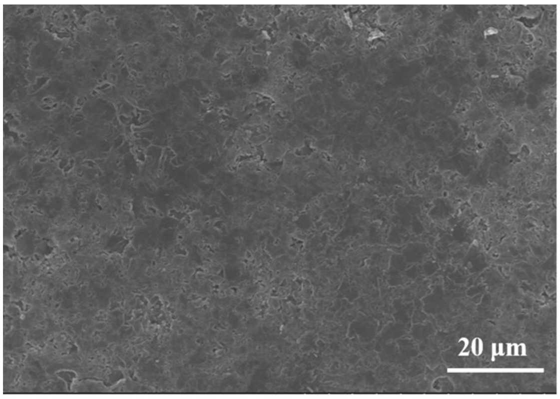

Fig. S17 Top view SEM image of Li foil after 1000 cycles in the Li/Li symmetric battery in ether-based electrolyte using C-3-modified PP separator at a current density of 1 mA/cm^2 with a cycling capacity of 1 mAh/cm^2.

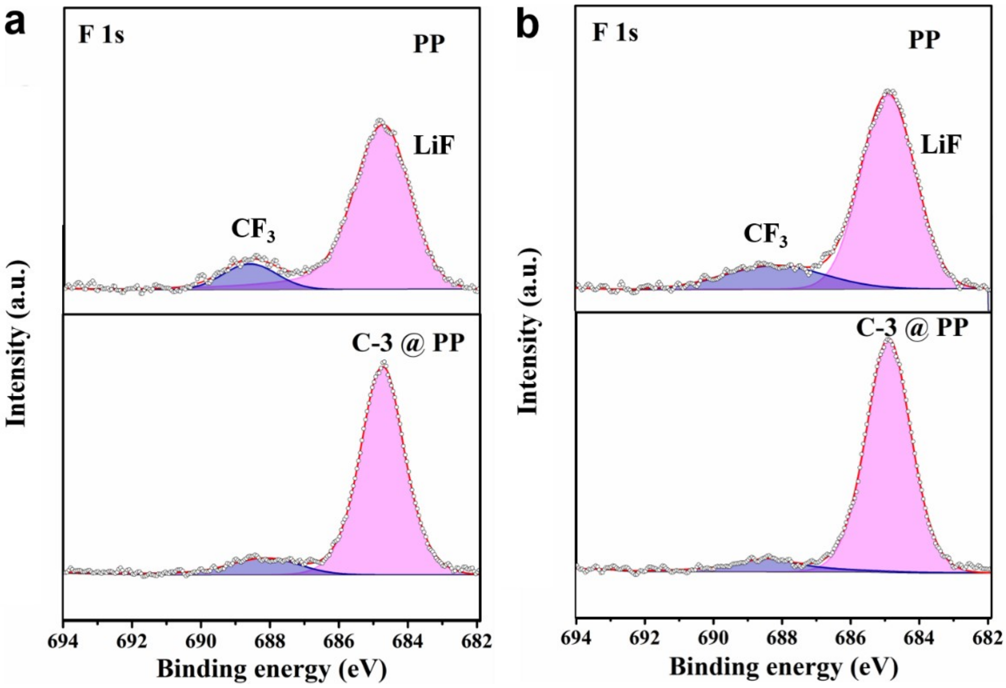

Fig. S18 XPS spectra of the SEI layers in ether-based electrolyte generated at different Ar sputtering time. F 1s spectra of the SEI layers using pristine PP and C-3-modified PP separators respectively after Ar sputtering for (a) 70 s and (b)105 s.

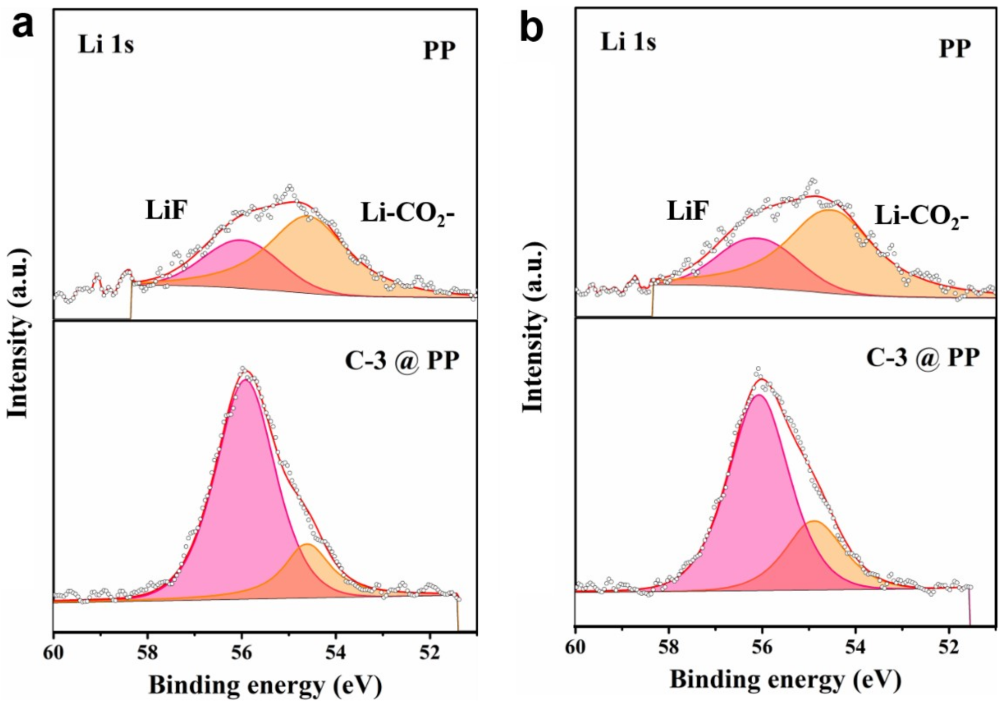

Fig. S19 XPS spectra of the SEI layers in ether-based electrolyte generated at different Ar sputtering time. Li 1s spectra of the SEI layers using pristine PP and C-3-modified PP separators respectively after Ar sputtering for (a) 70 s and (b) 105 s.

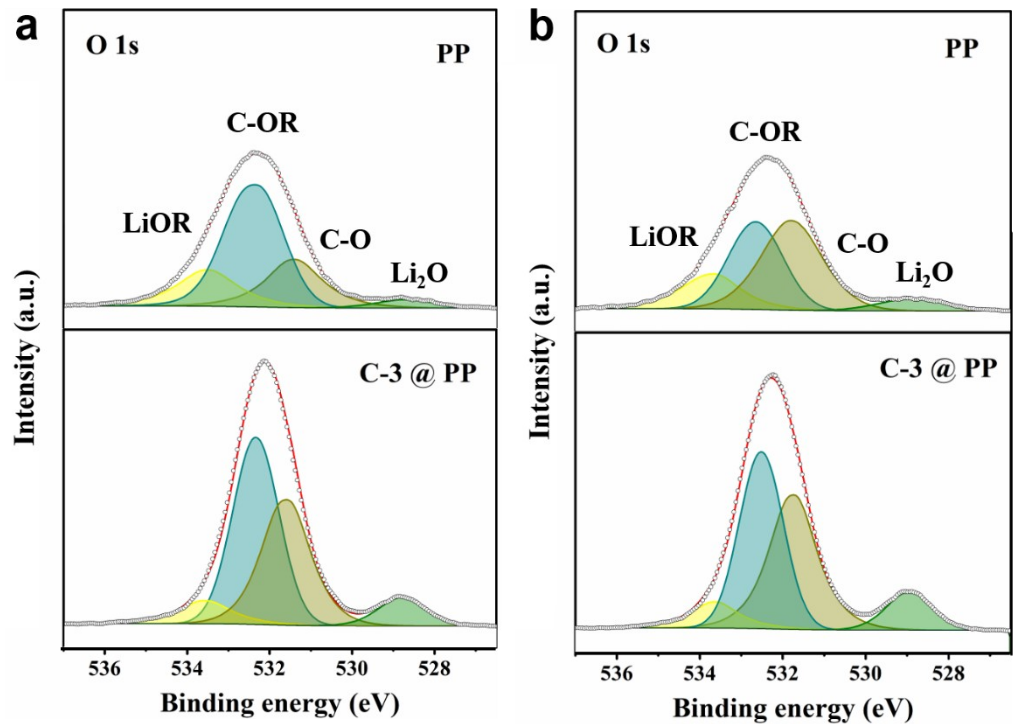

Fig. S20 XPS spectra of the SEI layers in ether-based electrolyte generated at different Ar sputtering time. O 1s spectra of the SEI layers using pristine PP and C-3-modified PP separators respectively after Ar sputtering for (a) 70 s and (b) 105 s.

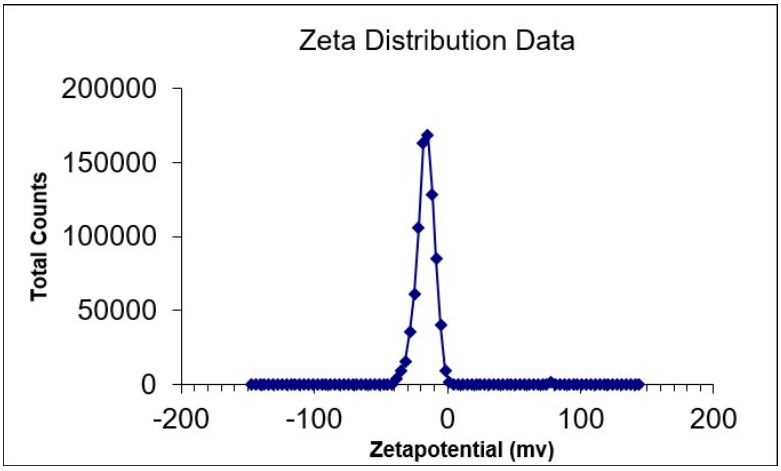

Fig. S21 Zeta potential of the polymer C-3.

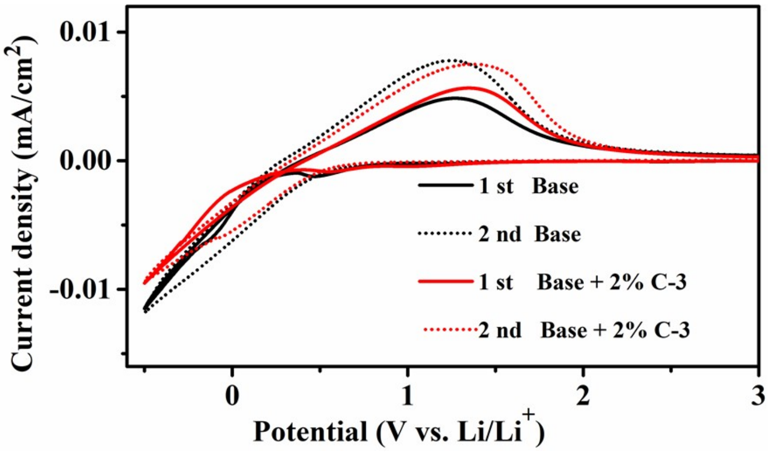

Fig. S22 CV curves of the Li/CP batteries in carbonate-based electrolyte in the first two cycles using the base electrolyte and electrolyte with 2 wt% C-3 as an additive, respectively.

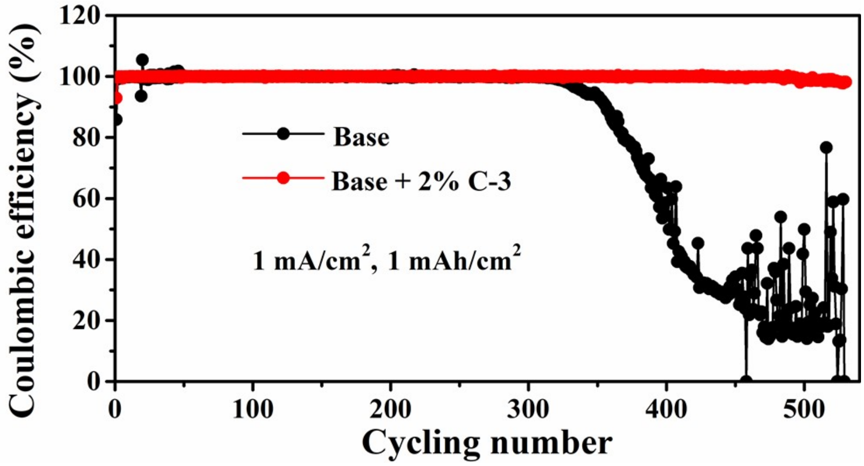

Fig. S23 Coulombic efficiency of the Li/CP batteries in carbonate-based electrolyte assembled with base and base + 2% C-3 electrolytes respectively at a current density of 1 mA/cm^2 with a cycling capacity of 1 mAh/cm^2.

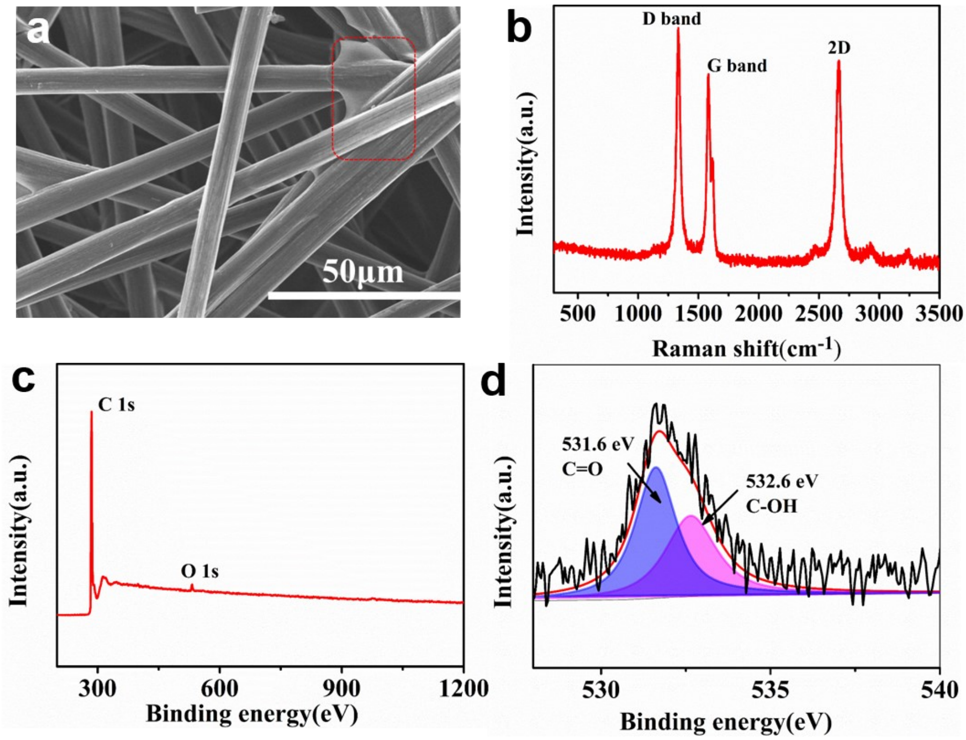

Fig. S24 (a) SEM image of carbon paper (CP) surface. (b) Raman analysis of CP. (c) Full XPS spectra of CP. (d) O 1s spectra of CP.

SEM image indicates that the CP is a cross-link framework composed of alternating carbon fibers (Fig. S24a). Meanwhile, Raman spectrum detects a D peak at 1331.4 cm^{-1}, a G peak at 1583.6 cm^{-1}, and a 2D peak at 2676.6 cm^{-1}, indicating that the CP has a graphene-like structure (Fig. S24b). XPS results show that there are two elements C and O on the CP surface (Fig. S24c). The peaks at 531.6 and 532.6 eV in the O 1s region belong to C=O and C-OH, respectively (Fig. S24d).

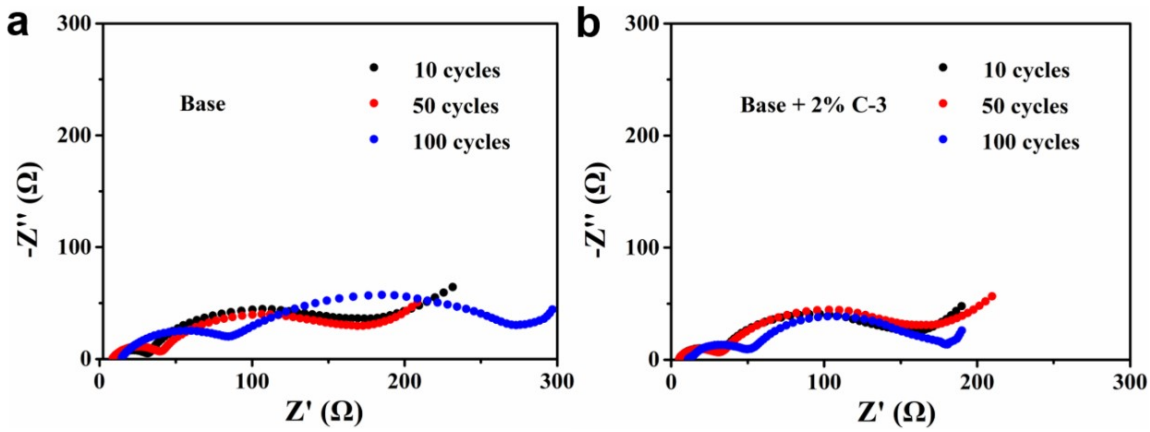

Fig. S25 Electrochemical impedance spectroscopy (EIS) results of Li/CP batteries in carbonate-based electrolyte assembled with (a) base electrolyte and (b) base + 2% C-3 electrolyte after 10, 50, and 100 cycles.

Section 2: Supplementary Tables

Table S1. Comparison of cycle life in symmetric batteries.

Modified SEI layer	Current density / cycle capacity (mA cm^{-2} / mAh cm^{-2})	Cycle life (hours)	Ref.
LiZn/Li_3PO_4	5/1	140	[1]
UiO-66-ClO_4	5/1	300	[2]
poly (vinyl alcohol)	5/2	200	[3]
hybrid polyurea layer	5/1	85	[4]
SEI enriched with LiF	5/5	600	[5]
LiF/Li_3Sb	5/5	600	[6]
polyacrylonitrile	5/1	300	[7]
Li_xSi alloy layer	5/1	1500	[8]
poly-melamine-formalde-hyde	5/1	80	[9]
3D Li-ion conductor	5/2.5	4000	[10]
anion-derived SEI	**5/2.5**	**12500**	**This work**

Table S2. Comparison of coulombic efficiency using 3D carbon-based hosts.

Electrode	Current density / cycle capacity (mA cm^{-2} / mAh cm^{-2})	Coulombic efficiency (%)	Cycle number	Ref.
cross-stacked carbon nanotube network/Li	1/1	99	300	[11]
ponge carbon layer on 3D carbon paper	0.5/3	98.5	150	[12]
porous carbon nanofibers	1/1	97	106	[13]
SiO_2/carbon-nanofibers composite skeleton	1/1	97.6	200	[14]
stacked graphene	0.5/1	97.1	200	[15]
nanoporous carbon tubes	0.5/0.5	96	200	[16]
carbon paper	**0.5/1**	**99.87**	**500**	**This work**
carbon paper	**1/1**	**99.78**	**550**	**This work**

Table S3. Comparison of the battery performance with low N/P ratio.

N/P ratio	Cycle rate (C)	Cycle number	Capacity retention (%)	Ref.
3	1	450	80	[5]
2	1/3	205	80	[17]
2	1/3	102	80	[18]
5	1/5	120	85	[19]
2.34	1/2	140	92.7	[20]
1.9		200	90.7	[21]
1.4	**1/2**	**400**	**86**	**This work**
1.4	**1**	**1000**	**90**	**This work**

Section 3: Supplementary References

1. X. Wang, J. Zhuang, M. Liu, C. Wang, Y. Zhong, H. Wang, X. Cheng, S. Liu, G. Cao and W. Li, *J. Mater. Chem. A*, 2019, **7**, 19104-19111.
2. G. Jiang, K. Li, F. Yu, X. Li, J. Mao, W. Jiang, F. Sun, B. Dai and Y. Li, *Adv. Energy Mater.*, 2021, **11**, 2003496.
3. H. Wu, Z. Yao, Q. Wu, S. Fan, C. Yin and C. Li, *J. Mater. Chem. A*, 2019, **7**, 22257-22264.
4. Y. Sun, M. Amirmaleki, Y. Zhao, C. Zhao, J. Liang, C. Wang, K. R. Adair, J. Li, T. Cui, G. Wang, R. Li, T. Filleter, M. Cai, T.-K. Sham and X. Sun, *Adv. Energy Mater.*, 2020, **10**, 2001139.
5. Y. Liu, X. Tao, Y. Wang, C. Jiang, C. Ma, O. Sheng, G. Lu and X. W. Lou, *Science*, 2022, **375**, 739-745.
6. A. Hu, W. Chen, X. Du, Y. Hu, T. Lei, H. Wang, L. Xue, Y. Li, H. Sun, Y. Yan, J. Long, C. Shu, J. Zhu, B. Li, X. Wang and J. Xiong, *Energy Environ. Sci.*, 2021, **14**, 4115-4124.
7. J. Bae, Y. Qian, Y. Li, X. Zhou, J. B. Goodenough and G. Yu, *Energy Environ. Sci.*, 2019, **12**, 3319-3327.
8. T. Xu, P. Gao, P. Li, K. Xia, N. Han, J. Deng, Y. Li and J. Lu, *Adv. Energy Mater.*, 2020, **10**, 1902343.
9. L. Fan, H. L. Zhuang, W. Zhang, Y. Fu, Z. Liao and Y. Lu, *Adv. Energy Mater.*, 2018, **8**, 1703360.
10. Z. Li, M. Peng, X. Zhou, K. Shin, S. Tunmee, X. Zhang, C. Xie, H. Saitoh, Y. Zheng, Z. Zhou and Y. Tang, *Adv. Mater.*, 2021, **33**, 2100793.
11. L. Ye, M. Liao, H. Sun, Y. Yang, C. Tang, Y. Zhao, L. Wang, Y. Xu, L. Zhang, B. Wang, F. Xu, X. Sun, Y. Zhang, H. Dai, P. G. Bruce and H. Peng, *Angew. Chem. Int. Ed.*, 2019, **58**, 2437-2442.
12. Z. Lu, Z. Zhang, X. Chen, Q. Chen, F. Ren, M. Wang, S. Wu, Z. Peng, D. Wang

and J. Ye, *Energy Stor. Mater.*, 2018, **11**, 47-56.
13. J. Cui, S. Yao, M. Ihsan-Ul-Haq, J. Wu and J.-K. Kim, *Adv. Energy Mater.*, 2019, **9**, 1802777.
14. Q. Song, H. Yan, K. Liu, K. Xie, W. Li, W. Gai, G. Chen, H. Li, C. Shen, Q. Fu, S. Zhang, L. Zhang and B. Wei, *Adv. Energy Mater.*, 2018, **8**, 1800564.
15. F. Ren, Z. Peng, M. Wang, Y. Xie, Z. Li, H. Wan, H. Lin and D. Wang, *Energy Stor. Mater.*, 2019, **16**, 364-373.
16. B. Moorthy, J.-H. Kim, H.-W. Lee and D. K. Kim, *Energy Stor. Mater.*, 2020, **24**, 602-609.
17. X. Cao, L. Zou, B. E. Matthews, L. Zhang, X. He, X. Ren, M. H. Engelhard, S. D. Burton, P. Z. El-Khoury, H.-S. Lim, C. Niu, H. Lee, C. Wang, B. W. Arey, C. Wang, J. Xiao, J. Liu, W. Xu and J.-G. Zhang, *Energy Stor. Mater.*, 2021, **34**, 76-84.
18. X. Ren, L. Zou, X. Cao, M. H. Engelhard, W. Liu, S. D. Burton, H. Lee, C. Niu, B. E. Matthews, Z. Zhu, C. Wang, B. W. Arey, J. Xiao, J. Liu, J.-G. Zhang and W. Xu, *Joule*, 2019, **3**, 1662-1676.
19. X.-Q. Zhang, X. Chen, X.-B. Cheng, B.-Q. Li, X. Shen, C. Yan, J.-Q. Huang and Q. Zhang, *Angew. Chem. Int. Ed.*, 2018, **57**, 5301-5305.
20. Y. Maeyoshi, D. Ding, M. Kubota, H. Ueda, K. Abe, K. Kanamura and H. Abe, *ACS Appl. Mater. Interfaces*, 2019, **11**, 25833-25843.
21. Y. Gao, Z. Yan, J. L. Gray, X. He, D. Wang, T. Chen, Q. Huang, Y. C. Li, H. Wang, S. H. Kim, T. E. Mallouk and D. Wang, *Nat. Mater.*, 2019, **18**, 384-389.